

Critical behavior of the  $n$ -component cubic model and the Ashkin-Teller fixed line

B. Nienhuis,\* E. K. Riedel,<sup>†</sup> and M. Schick

*Department of Physics, University of Washington, Seattle, Washington 98195*

(Received 17 December 1982)

The cubic lattice gas, a generalization of the  $n$ -component face-cubic model, is studied in two dimensions by variational renormalization-group techniques for general  $n$ , and by an exact mapping onto a solid-on-solid model for  $n=2$ . This approach reveals new interconnections among the class of cubic, Potts, and Ashkin-Teller phase-transition phenomena. In particular, it is shown that the fixed line of the Ashkin-Teller lattice gas serves as the backbone for a hierarchy of pairs of fixed points which branch off from it, as  $n$  is decreased from 2, at special points where two operators are marginal. The phase diagrams of the pure and dilute  $n$ -component cubic models are obtained and the orders of all transitions are determined. The cubic phase transition is found to be first order for all  $n > n_c = 2$ . The evolution of the results as a function of dimensionality is discussed briefly.

I. INTRODUCTION

Because the cubic model contains as special cases the Potts and Ashkin-Teller (AT) models, it is not surprising that it exhibits a complex phase-transition behavior and has resisted a satisfactory renormalization-group (RG) description. Motivated by the recent successful calculation of the properties of the Potts model,<sup>1,2</sup> we have applied similar methods to this problem in conjunction with exact mapping techniques. We obtain an RG description which is not only satisfactory, but also reveals new interconnections between two-dimensional phase-transition phenomena in which the AT fixed line plays a central role.<sup>3</sup> Most of our calculations concern the cubic model in two dimensions, but the evolution of the results as a function of dimension is briefly discussed.

The  $n$ -component cubic model can be defined in several ways. The usual definition<sup>4</sup> is by a Hamiltonian containing two nearest-neighbor interactions between  $n$ -component spins  $\vec{S}$  that point to the faces of an  $n$ -dimensional hypercube,  $\vec{S} = (\pm 1, 0, \dots)$ ,  $(0, \pm 1, 0, \dots)$ ,  $\dots$ ,

$$-\beta\mathcal{H} = \sum_{\langle i,j \rangle} \left\{ \frac{1}{2} C (\vec{S}_i \cdot \vec{S}_j - 1) + \left( \frac{1}{2} C + P \right) [(\vec{S}_i \cdot \vec{S}_j)^2 - 1] \right\}, \quad (1.1)$$

where the sum is over all nearest-neighbor pairs. This model is also called the face-cubic or axis model and should be distinguished from the corner-cubic or diagonal model, in which the spins point to the corners of an  $n$ -dimensional hypercube. The Hamiltonian (1.1) can be rewritten in a form that makes more obvious its important symmetry proper-

ties. We associate two discrete variables with each lattice site  $i$ : The "axis" variable  $a_i = 1, \dots, n$  that determines which component of  $\vec{S}_i$  is nonzero and an Ising variable  $\sigma_i = \pm 1$  that determines the sign of that component. In terms of these variables the cubic model is defined by

$$-\beta\mathcal{H} = \sum_{\langle i,j \rangle} [C(\delta_{a_i, a_j} \delta_{\sigma_i, \sigma_j} - 1) + P(\delta_{a_i, a_j} - 1)]. \quad (1.2)$$

For  $P=0$  the Hamiltonian reduces to the  $2n$ -state Potts model,<sup>5</sup> and for  $n=2$  it specializes to the AT model.<sup>6</sup> It is convenient to describe the parameter space in terms of the Boltzmann weights for pairs of antiparallel and orthogonal spins, respectively:

$$W_{\uparrow\downarrow} = \exp(-C), \quad W_{\uparrow\rightarrow} = \exp(-C - P). \quad (1.3)$$

The Boltzmann weight for parallel spins is unity by construction. We consider only the ferromagnetic sector of the parameter space, which is given by

$$0 < W_{\uparrow\downarrow}, W_{\uparrow\rightarrow} < 1. \quad (1.4)$$

Often the term cubic model is applied to the continuous-spin Landau Hamiltonian<sup>7</sup>

$$-\beta\mathcal{H}_L = \int d^d x \left[ \frac{1}{2} |\vec{\nabla} \vec{\psi}|^2 + r \vec{\psi}^2 + u |\vec{\psi}^2|^2 - v \sum_{\alpha} \psi_{\alpha}^4 + \dots \right], \quad (1.5)$$

where  $\vec{\psi}$  is an  $n$ -component variable. The quartic term  $v \sum_{\alpha} \psi_{\alpha}^4$  breaks the isotropic symmetry, favoring spin orientations toward the faces or corners of an  $n$ -dimensional hypercube for  $v < 0$  or  $v > 0$ , respectively. This Hamiltonian thus describes both face- and corner-cubic transitions, and elucidates

their relation to the isotropic or  $O(n)$  transition; however, it exhibits only one of the several transitions of the model (1.1).<sup>8,9</sup>

The cubic model in two dimensions has many applications, in particular to adsorbed monolayers.<sup>10</sup> For example, with  $n=3$  the model describes the orientational ordering of diatomic molecules adsorbed in a triangular array,<sup>11</sup> as observed in the  $N_2$ -graphite system,<sup>12</sup> and the magnetic ordering of planar spins adsorbed in a triangular lattice,<sup>13</sup> as observed in the  $O_2$ -graphite system<sup>14</sup>; with  $n=2$ , the model describes the transition to  $(2 \times 1)$  structures on centered-rectangular arrays,<sup>13,15</sup> as in O on Ni(110) (Ref. 16); with  $n=1$  the model describes the transition to  $(1 \times 1)$  ( $\frac{1}{2}$ ) structures on honeycomb arrays,<sup>17</sup> as in He on Kr-plated graphite.<sup>18</sup> The limit  $n=0$  describes the scaling behavior of long polymer chains,<sup>19</sup> which have also been studied experimentally<sup>20</sup> in two dimensions.

With the parameter space restricted as in (1.4), the cubic model exhibits three phases. In the ferromagnetic phase, which occurs for  $C$  sufficiently large, all spins tend to align so that  $\langle \vec{S} \rangle \neq 0$ . When  $C$  and  $P$  are small or about equal and opposite, the model is in a paramagnetic or disordered phase. In a third phase, which occurs at large positive  $P$  and small  $C$ , the spins exhibit partial order in the sense that they all point along one axis, but do not favor either of the two directions along the axis. The reader may view Fig. 1(a) as a generic phase diagram, ignoring all details since they will be discussed later. From symmetry considerations the transition between the partially and fully ordered phases is expected to be in the Ising universality class. For the same reasons the transition from the paramagnetic to the partially ordered phase is an  $n$ -state Potts transition. These conclusions are obvious in the following special cases. In the limit  $P \rightarrow \infty$  the axis variables are all equal and the cubic model reduces to an Ising model. When  $C=0$ , the Ising variables do not interact. This leaves only an  $n$ -state Potts transition. The nature of this transition is known to be second order for  $n \leq 4$  and first order for  $n > 4$ .<sup>21</sup> Now consider the single paramagnetic-to-ferromagnetic transition. It will be referred to as the "cubic" transition when  $P < 0$ . For  $P=0$ , the cubic model reduces to a  $2n$ -state Potts model. Hence for all values of  $n$  there is a single phase transition at  $P=0$ , which changes from second to first order with increasing  $n$  at  $n=2$ . For this value of  $n$  the cubic model is identical with the AT model. The AT critical line with continuously varying exponents is located at  $P < 0$ , and splits into two Ising-transition lines at the four-state Potts point  $P=0$ .<sup>22</sup>

A question left open by previous work is the nature of the cubic transition.<sup>8,23</sup> Because the  $2n$ -state

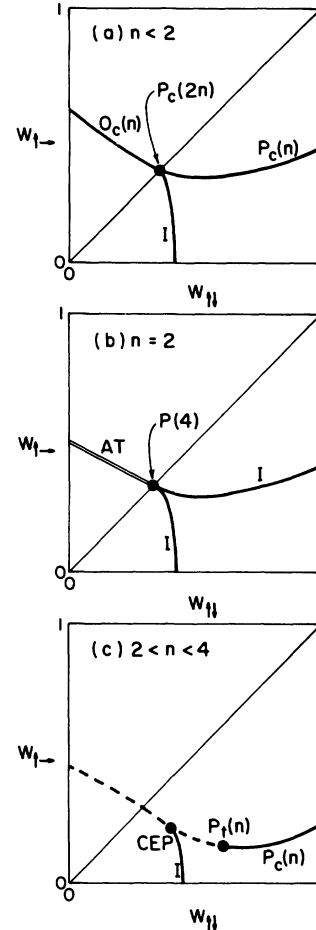


FIG. 1. Schematic phase diagrams of the  $n$ -component cubic model for (a)  $n < 2$ , (b)  $n = 2$ , and (c)  $2 < n < 4$  exhibiting isotropic  $n$ -vector  $O_c$ ; Ashkin-Teller AT;  $n$ - and  $2n$ -state Potts critical and tricritical  $P_c, P_t$ ; Ising  $I$ ; and critical end-point (CEP) transitions. The axes are labeled by the Boltzmann weights  $W_{\uparrow\rightarrow}$  and  $W_{\uparrow\parallel}$  defined in Eq. (1.3). Solid and dashed lines denote continuous and first-order phase transitions, respectively. The double line indicates the AT transitions with continuously varying critical exponents. For  $n > 4$  the entire  $n$ -state Potts transition line is also first order.

Potts transition is first order for  $n > 2$  we expect, by continuity, the cubic transition in the neighborhood of  $P=0$  to be first order. However, for sufficiently negative  $P$  the cubic transition could remain continuous either for all  $n$  or up to some  $n_c$  beyond which it is first order everywhere. In either case it is clear that the change in the nature of the  $2n$ -state Potts transition must cause an evolution of the cubic transition with  $n$ . The bifurcation point of the cubic transition into  $n$ -state Potts and Ising transitions must also be affected, becoming a bicritical point, a critical end point, or a triple point.

For several reasons it is useful to study these and other questions by means of a generalization of the cubic model (1.2) to the dilute cubic model or cubic lattice gas. The nearest-neighbor Hamiltonian for this system is

$$-\beta\mathcal{H} = \sum_{\langle i,j \rangle} t_i t_j [K + C(\delta_{a_i, a_j} \delta_{\sigma_i, \sigma_j} - 1) + P(\delta_{a_i, a_j} - 1)] - \Delta \sum_i t_i, \quad (1.6)$$

where the variables  $t_i$  specify whether a site  $i$  is occupied ( $t_i = 1$ ) or vacant ( $t_i = 0$ ). The number of vacancies is controlled by the chemical potential  $\Delta$  and the lattice-gas coupling  $K$ . The model (1.6) describes an even greater variety of phase-transition behaviors than (1.2). A transition that is continuous in the pure cubic model can be driven first order by a sufficient amount of dilution. The dilute model also covers a wider range of applications and may be of interest, for example, for monolayer experiments in which coverage can be easily varied. Finally, there are technical reasons for investigating the dilute rather than the pure cubic model.<sup>1</sup> Allowing vacancies to *develop* under RG transformations enables one to use the usual approximate RG methods to obtain subtle features such as the AT fixed line and changeover between continuous and first-order phase transitions.

The purpose of this paper is to report results for the cubic-lattice-gas model obtained, for general  $n$ , by the variational RG and, in the AT limit,  $n=2$ , also by mapping onto a solid-on-solid model. A summary of these results follows.

First, the cubic transition for  $n > n_c = 2$  is first order for all  $P < 0$ . For  $n < n_c$  it exhibits critical, tricritical, or first-order behavior depending on the degree of dilution. The critical point is in the universality class of the  $O(n)$  transition. The tricritical exponents are those of the  $2n$ -state Potts lattice gas. The AT tricritical behavior, unlike the critical behavior, is universal and four-state Potts-type.

Second, the point at which the cubic transition splits into  $n$ -state Potts and Ising branches evolves with  $n$  in the following manner. For  $n < 2$ , this point is the  $2n$ -state Potts critical point as long as the transition is continuous; when the cubic transition is driven first order by dilution the splitting occurs at a bicritical point at  $P > 0$  with the exponents of the  $2n$ -state Potts tricritical point. At  $n=2$  this bicritical point is found to exhibit nonuniversal exponents with varying dilution. For  $n > 2$ , where the cubic transition is always first order, our results indicate that the point of splitting is an Ising critical end point. However, due to the

character of our calculation, we cannot exclude that it is an  $n$ -state Potts critical end point or a triple point.

Third, our conclusions as to the interconnections between the above-mentioned phase transitions are summarized in Fig. 3. The thermal exponents associated with the isotropic  $n$ -vector, critical and tricritical Potts, and new multicritical transition  $A$  are shown as functions of  $n$ . The vertical line at  $n=2$  represents the continuous variation of the AT thermal exponent along the AT fixed line. All of the exponents shown, with the exception of the multicritical one,  $A(n)$ , are known exactly. Our mapping of the AT lattice onto a solid-on-solid model establishes that for this model the fixed line consists of a sequence of segments with an increasing degree of instability. We conclude that the points at which this extended AT fixed line changes stability, i.e.,  $y_t = 0, \frac{3}{2}, \frac{16}{9}, \frac{15}{8}, \dots$ , are bifurcation points at which pairs of fixed lines branch off as functions of  $n$  for  $n < 2$ , which describe isotropic, Potts, and multicritical phase transitions. As suggested by the figure, we refer to the AT fixed line as the “backbone” for the phase transitions exhibited by the cubic lattice gas.

Fourth, the calculation produces the topology of the RG phase diagram of the cubic lattice gas as function of  $n$ , as summarized in Fig. 2 below. The evolution with  $n$  of the pure cubic phase diagram, inferred from this information, is shown in Fig. 1.

Fifth, though most of the calculations are done for the two-dimensional model, some conclusions can be drawn concerning the cubic model in dimensions greater than 2.

The outline of this paper is as follows. Section II discusses the Kadanoff variational RG as applied to the cubic model. Some technical details are presented in Appendix B. Section III presents the results of the RG calculation and the conclusions drawn from them. The numerical results are interpreted with the aid of several exact results, some of which are new and follow from a mapping of the AT lattice gas onto a solid-on-solid model. The consequences of this mapping are discussed in Sec. III, while the mapping itself is presented in Appendix A.

## II. METHODS

This section gives a brief summary of the techniques applied in the present study. Details are deferred to Appendixes A and B.

The RG approach presented here embeds the cubic model (1.2) in the enlarged parameter space of a cubic lattice gas (1.6). This has calculational advantages besides making accessible a greater variety of

phase-transition problems. First, a central point in the phase diagram of the cubic model is the  $2n$ -state Potts transition at  $P=0$ , which is continuous for  $n < q_c/2$  and first order for  $n > q_c/2$ , with  $q_c=4$  in two dimensions.<sup>21</sup> This changeover has been described within an approximate RG calculation by allowing vacancies to be generated under the transformation as a means of representing disordered Potts-spin configurations.<sup>1,2</sup> The introduction of the vacancy or dilution concept into the discussion of the Potts model has been very successful. The phenomenological picture that resulted, i.e., of merging lines of critical and tricritical Potts fixed points along which the dilution operator becomes marginal as  $n \rightarrow q_c/2$ , has been confirmed by subsequent analytical calculations.<sup>24</sup> The latter works also revealed that the singly and doubly unstable segments of the Gaussian fixed line are related to and control the critical and tricritical Potts behavior, respectively, which explains the extended den Nijs conjecture<sup>1,25</sup> for the thermal exponent of the Potts model.

The second reason for the extension (1.6) requires a more detailed explanation, which is given partly here and partly in Appendix A. When  $n=2$ , the Hamiltonian (1.2) defines the AT model that is known to exhibit a phase diagram of the kind<sup>22</sup> shown in Fig. 1(b) with, for  $P < 0$ , a thermal exponent that varies continuously as a function of  $P/C$ .<sup>26</sup> This AT fixed line<sup>27</sup> terminates, when  $P=0$ , in a point of four-state Potts symmetry. The thermal exponent of the AT model can be associated with the relevant operator of the Gaussian model,  $\cos(2\pi h)$ .<sup>28,29</sup> For definitions and details see Appendix A. When the parameter  $P$  becomes positive, the Gaussian operator  $\cos(4\pi h)$  also becomes relevant, so that flows from the AT model no longer reach the Gaussian fixed line. An approximate calculation yields this termination only if it includes the equivalent of the operator  $\cos(4\pi h)$ . We achieve this by working in the extended Hamiltonian space (1.6), as is shown in Appendix A and discussed in Sec. III. Therefore, introducing the dilution operator is a device that allows one to capture within an approximate RG calculation the essential physics of the cubic model.

Specifically, the cubic lattice gas (1.6) in two dimensions is investigated by Kadanoff's variational RG.<sup>30</sup> Details of the approach are described in Appendix B. In this scheme the Hamiltonian is a sum of local Hamiltonians each representing the  $2^d$  sites of an elementary hypercube in  $d$  dimensions,  $-\beta\mathcal{H} = \sum H_{hc}$ . For the cubic lattice gas in two dimensions this involves 21 coupling constants associated with the 21 energetically different configurations of  $\{t, a, \sigma\}$  on a square. The calculation of the

renormalized Hamiltonian requires an approximation which is constructed such that the resulting free energy is a lower bound to the exact free energy. The calculation is then optimized with respect to four parameters by maximizing this lower bound. The approach is known to yield excellent results for the critical and tricritical exponents of the Potts model,<sup>2</sup> which are now known exactly.<sup>24</sup> It has the minor disadvantage, in particular when fixed points in large parameter spaces must be located, that it does not allow the construction of RG flows. However, in the present calculation we found it possible to start from well-identified fixed points at certain values of  $n$  and to generate lines of fixed points as functions of  $n$  by changing  $n$  in small steps. Our results are described in Sec. III.

The interpretation of the numerical results of the RG calculation is guided by a number of exact results, which will be addressed in more detail later. For now we note the following.

(1) The line of  $2n$ -state Potts critical points and the AT fixed line have the four-state Potts fixed point in common. At this intersection the  $2n$ -state Potts transition changes from continuous to first order,<sup>21</sup> and the line of AT critical points bifurcates<sup>22</sup> into two Ising transitions. The thermal critical and tricritical Potts exponents are known exactly.<sup>24</sup>

(2) At the isotropic  $n$ -vector critical point the cubic anisotropy is irrelevant for  $n < 2$ .<sup>7,31,32</sup> This implies that at least for some range of interactions the cubic transition is in the  $O(n)$  universality class for these values of  $n$ . The AT and  $O(n)$  lines of fixed points intersect at  $n=2$ .<sup>28,29,33</sup> The thermal exponent of the  $O(n)$  transition is known exactly.<sup>34</sup>

(3) The AT lattice gas exhibits a fixed line which has not only a singly unstable segment as in the pure AT model, but also a doubly unstable segment. This result follows from a mapping of the AT lattice gas onto a solid-on-solid model, which is presented in Appendix A. The thermal exponent along the AT fixed line is also known exactly.<sup>26,28</sup>

### III. RESULTS

Our conclusions as to the structure of the phase diagram of the two-dimensional cubic lattice gas are presented in Sec. IIIA below. The evolution with  $n$  of the fixed points which govern the phase-transition behavior is discussed in Sec. IIIB and leads to the conclusion that the AT fixed line plays a special role, tying together these disparate transitions. These conclusions are based on the results of our approximate RG calculations, presented in Sec. IIIC, and on the exact mapping of the AT lattice gas onto a solid-on-solid model, carried out in Ap-

pendix A. In Sec. III D we comment on the evolution with dimensionality of some of our results.

### A. Phase diagram

Figures 2(a)–2(c) summarize our conclusions concerning the phase diagrams of the cubic lattice gas in the parameter space of the Boltzmann weights (1.3) and the fugacity  $\exp(\Delta)$ . The intersection of the pure, or zero-fugacity, plane with the various transition surfaces produces the phase diagrams of the pure cubic model shown in Figs. 1(a)–1(c). Qualitative differences exist between the diagrams for  $n < 2$ ,  $n = 2$ ,  $2 < n < 4$ , and  $n > 4$ . In all cases there is a single cubic transition between the paramagnetic and ferromagnetic phases at  $P < 0$ ; this transition bifurcates into  $n$ -state Potts and Ising transitions at  $P = 0$  or  $P > 0$ , depending on the values of  $n$  and dilution. The details are as follows.

For  $n < 2$ , the cubic transition surface ( $P < 0$ ) in Fig. 2(a) has first- and second-order regions that are separated by a tricritical line. The continuous transition is governed by the singly unstable isotropic fixed point  $O_c(n)$  located at  $P < 0$ . (Our reasons for identifying this transition with the isotropic rather than cubic universality class are given in Secs. III B and III C.) Its thermal exponent as a function of  $n$ , which is given by Eq. (3.2) below,<sup>34,35</sup> is indicated in Fig. 3. The transition line in the Potts subspace  $P = 0$  is controlled by the critical, tricritical, and discontinuity  $2n$ -state Potts fixed points  $P_c(2n)$ ,  $P_t(2n)$ , and  $P_d(2n)$ . The discontinuity fixed point  $P_d(2n)$  is stable against cubic anisotropy so that for large dilution the single or cubic transition is first order for  $P < 0$  and also for some region  $P > 0$ , into which it then extends. The critical fixed point  $P_c(2n)$  is stable in the dilution direction and unstable under cubic symmetry breaking. The continuous cubic transition surface for weak dilution splits at  $P = 0$ , along the line governed by  $P_c(2n)$ , into the  $n$ -state Potts and Ising surfaces. At the tricritical fixed point  $P_t(2n)$  dilution is relevant and cubic anisotropy is irrelevant. Consequently, this fixed point governs the cubic and  $2n$ -state Potts tricritical transitions for  $P \leq 0$  and a bicritical line for  $P > 0$ . The latter is the line along which the first-order paramagnetic-to-ferromagnetic transition bifurcates into continuous  $n$ -state Potts and Ising transitions for large dilution. Figure 2(a) clearly exhibits this role of the fixed point  $P_t(2n)$ . The thermal exponents associated with  $P_c(2n)$  and  $P_t(2n)$  are given by Eq. (3.1) below<sup>24</sup>; their dependence on  $n$  is shown in Fig. 3. Large dilution also drives to first order the transition on the  $n$ -state Potts surface; then the bifurcation exhibits critical-end-point behavior and is controlled by the fixed-point CEP. The special

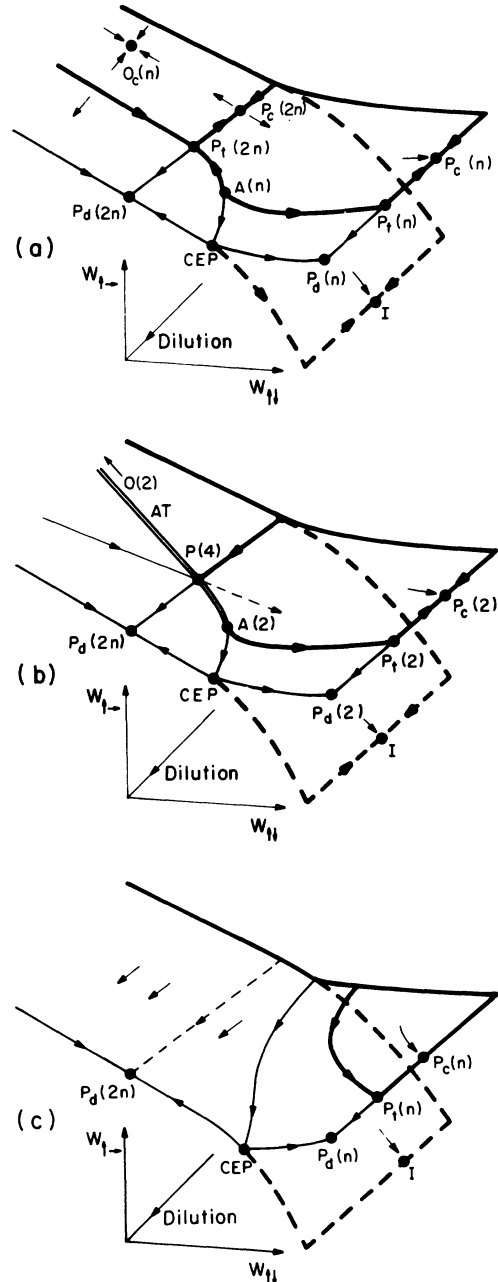


FIG. 2. Schematic phase diagram of the cubic-lattice-gas model for (a)  $n < 2$ , (b)  $n = 2$ , and (c)  $2 < n < 4$ . The surfaces separate disordered, partly ordered, and fully ordered regions with decreasing  $W_{I\to}$ . The fixed points are denoted as follows:  $O_c$ , isotropic  $n$  vector;  $P_c$ , Potts critical;  $P_t$ , Potts tricritical;  $P_d$ , Potts discontinuity; CEP, critical end point;  $A$ , multicritical; and  $I$ , Ising. The double line is the Ashkin-Teller fixed line, of which the segment  $P(4)$  to  $A(2)$  is doubly unstable. The AT tricritical behavior is controlled by  $P(4)$ ; the dashed flow line emerging from  $P(4)$  lies between the two-state Potts and Ising surfaces. The discontinuity fixed points  $P_d$  control first-order phase transitions.

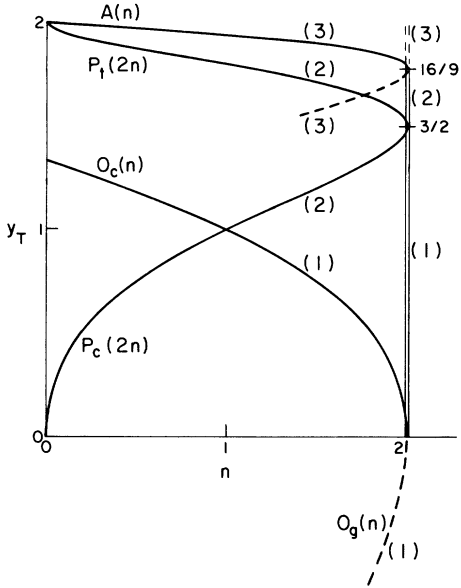


FIG. 3. Thermal critical exponents vs  $n$  of isotropic  $n$ -vector,  $2n$ -state Potts, and multicritical fixed points. The curves are labeled as follows:  $O_c(n)$  and  $O_g(n)$ , the isotropic  $n$ -vector critical and low-temperature fixed points;  $P_c(2n)$  and  $P_t(2n)$ , the  $2n$ -state Potts critical and tricritical fixed points, and  $A(n)$  the multicritical point governing crossover from bicritical to critical-end-point behavior [see Fig. 2(a)]. The double vertical line at  $n=2$  represents the continuously varying AT exponents. The numbers in parentheses indicate the number of relevant fields at each of the fixed points. Along the AT line there is also one marginal operator. The dashed curves indicate the exponents of fixed points that are not accessible in the cubic-lattice-gas calculation. The dashed curve labeled (3) is associated with the fixed point denoted  $B(n)$  in the text. The  $A(n)$  exponents shown are schematic, but of the other exponents the exact values are plotted.

point at which the nature of the bifurcation changes from bicritical to critical-end-point behavior is attracted by the triply unstable fixed point  $A(n)$ . The thermal exponent of  $A(n)$  is shown schematically in Fig. 3. The critical, tricritical, and first-order behavior of the  $n$ -state Potts surface is governed by the fixed points  $P_c(n)$ ,  $P_t(n)$ , and  $P_d(n)$ , respectively. The Ising-transition surface is continuous everywhere and is controlled by the fixed point  $I$ . That the Ising sheet does not display first-order and tricritical transitions is probably a bias of our calculation. We will return to this point in Sec. III C and Appendix A.

Figure 2(b) exhibits the RG phase diagram for  $n=2$ , or the AT lattice gas. It looks very similar to the phase diagram for  $n < 2$ , but three changes have occurred that pertain to the nature of the phase

transitions: The fixed point  $O_c(n)$  has moved to  $P = -\infty$ ; the fixed points  $P_c(2n)$  and  $P_t(2n)$  have merged into one fixed point, labeled  $P(4)$ ; and, most importantly, a line of fixed points has appeared. This fixed line, which is indicated by a double line in the figure, is the “extended” fixed line of the AT lattice gas. The segment  $O(2)$  to  $P(4)$  is singly unstable (in the temperature direction) and marginal under cubic anisotropy, while the segment  $P(4)$  to  $A(2)$  is doubly unstable (in temperature and dilution) and marginal in the cubic anisotropy. The singly unstable segment controls the second-order AT or cubic transition, which has a thermal exponent  $y_T$  that varies as a function of  $P/C$  from 0 to  $\frac{3}{2}$ . The doubly unstable segment describes a bicritical transition with two continuously varying relevant exponents,  $\frac{3}{2} < y_T < \frac{16}{9}$  and  $0 < y_{T,2} < \frac{10}{9}$ , from  $P(4)$  to  $A(2)$ . The derivation of the exponent values is discussed in Sec. III B [see Eqs. (3.3) and (3.4)]. The variation of the AT thermal exponent is indicated in Fig. 3 by the vertical double line at  $n=2$ . The AT tricritical transition at  $P < 0$  is controlled by  $P(4)$  and therefore is universal in contrast to the AT critical behavior.  $P(4)$  also governs the part of the  $P=0$  line along which the continuous AT transition bifurcates. This unusual flow pattern is possible because  $P(4)$  has two marginal operators. The rest of the phase diagram at  $n=2$  is qualitatively identical to that for  $n < 2$ .

The phase diagram for  $2 < n < 4$  shown in Fig. 2(c) has much less structure. The fixed points  $O_c(n)$ ,  $P_c(2n)$ ,  $P_t(2n)$ , and  $A(n)$  have disappeared. The cubic transition, governed by  $P_d(2n)$ , is now first order everywhere. This first-order transition surface splits into  $n$ -state Potts and Ising sheets along a line of critical end points at  $P > 0$ , which is controlled by the CEP. Near this line the  $n$ -state Potts transition is first order as well. However, for small dilution and sufficiently far from the critical end point the  $n$ -state Potts transition is continuous. The Ising sheet remains second order and is controlled by the fixed point  $I$ .

When  $n=4$ , the fixed points  $P_c(n)$  and  $P_t(n)$  of Fig. 2(c) meet and annihilate. Consequently, for  $n > 4$ , the  $n$ -state Potts surface is first order everywhere and is governed by  $P_d(n)$ . The Ising transition remains continuous. Hence, for  $n > 4$ , the phase diagram is essentially independent of dilution.

### B. Model interconnections

In this section it is shown that the fixed points that determine the phase structure of the cubic lattice gas occur in pairs. As  $n$  approaches 2 from below, the fixed-point pairs annihilate at special points of the extended AT fixed line, where it

changes stability. Thus the AT fixed line is the unifying element of these disparate fixed-point behaviors. The results in Fig. 3 for the thermal exponents of the various fixed points indicate this role of the AT fixed line.

Consider first the most familiar of these fixed-point pairs, the  $2n$ -state Potts critical and tricritical fixed points  $P_c(2n)$  and  $P_t(2n)$  that are both twofold unstable. The relevant operators of  $P_c(2n)$  are temperature and cubic anisotropy, and those of  $P_t(2n)$  are temperature and dilution. As  $n$  approaches 2 these two fixed points coalesce and simultaneously meet the AT fixed line at  $P(4)$ . At the same point the AT line changes from singly to doubly unstable. Both dilution and cubic anisotropy are marginal at  $P(4)$ . The thermal exponents of  $P_c(2n)$  and  $P_t(2n)$  have been calculated exactly<sup>24</sup>:

$$y_{T,P} = 3 \left[ 1 - \left[ 2 \pm \frac{1}{\pi} \cos^{-1}(n-1) \right]^{-1} \right], \quad (3.1)$$

where the plus and minus signs refer to the tricritical and the critical transition, respectively.

Next consider the cubic lattice gas at the continuous cubic transition. The discrete face-cubic spins can be regarded as isotropic  $n$ -component spins in a field which forces them to point to the faces of a hypercube. Under an exact RG transformation this field is expected to diminish, so that the cubic model renormalizes into an  $O(n)$  model, when  $n < 2$ . The critical behavior of the two-dimensional  $O(n)$  model has become better understood recently.<sup>34</sup> The model has a critical fixed point  $O_c(n)$  controlling the phase transition and a low- (but finite) temperature fixed point  $O_g(n)$  governing the isotropic low-temperature phase. The fixed point  $O_c(n)$  is stable under cubic anisotropy, as indicated above, but unstable in the temperature direction. In the low-temperature phase, however, the isotropic and cubic spin models are very different. The  $O(n)$  model has Goldstone modes in the low-temperature phase and the cubic model does not. Therefore, at  $O_g(n)$  the cubic anisotropy is relevant, while the temperature is irrelevant. The thermal exponents of  $O_c(n)$  and  $O_g(n)$  have been calculated and are given by<sup>34</sup>

$$y_{T,O} = 4 \left[ 1 - \left[ 1 \pm \frac{1}{\pi} \cos^{-1}(n/2) \right]^{-1} \right], \quad (3.2)$$

where the plus sign refers to  $O_c(n)$  and the minus sign to  $O_g(n)$ . As  $n$  approaches 2,  $O_c(n)$  and  $O_g(n)$  coalesce and disappear, which indicates the absence of a finite-temperature phase transition for  $O(n > 2)$  models. At  $n=2$ , where  $O_c(n)$  and  $O_g(n)$  coincide on the AT line,<sup>33</sup> both temperature and cubic anisotropy are marginal. In Fig. 3 the thermal eigenvalue

of  $O_g(n)$  is indicated by the dashed line at the bottom. The scenario is remarkably similar to the behavior of  $P_c(2n)$  and  $P_t(2n)$ : Two fixed points of equal degree of instability, located in a subspace of special symmetry, coalesce the AT fixed line, where they exchange relevant operators. At the special point at which the fixed points coincide with the AT line there are two marginal operators.

Now consider the AT line in more detail. As shown in Appendix A, the AT lattice gas can be mapped onto a solid-on-solid model. The critical behavior of such models is that of a Gaussian model with a hierarchy of spin-wave fields.<sup>28,29</sup> The temperature of the original AT lattice gas is related to the most relevant spin-wave operator. Its exponent is known for the pure AT model,<sup>26</sup> e.g., on the square lattice

$$y_1 = 2 - \left[ 2 - \frac{4}{\pi} \cos^{-1} \left( \frac{e^P + 1}{2} \right) \right]^{-1}, \quad (3.3)$$

which defines the thermal AT exponent  $y_{T,AT} \equiv y_1$  for this lattice. The exponent varies along the line of critical points given by

$$\exp(C) = 1 + 2 \exp(-P).$$

The less relevant exponents can be expressed in terms of the thermal exponent<sup>28</sup>

$$y_k = 2 - k^2(2 - y_1), \quad (3.4)$$

for  $k = 1, 2, \dots$ . As  $y_1$  increases, more operators become relevant.

The  $O(n)$  fixed points meet the AT line at the point where  $y_1 = 0$ . The  $2n$ -state Potts fixed points intersect with the AT line at  $P(4)$ , where  $y_2 = 0$  and  $y_1 = \frac{3}{2}$ . We argue that the fixed point  $A(n)$  exhibits a similar behavior. In an appropriately enlarged parameter space there is another threefold unstable fixed point  $B(n)$ . As  $n$  approaches 2,  $A(n)$  and  $B(n)$  coalesce at the AT line and exchange stability in one of their operators. At that point  $y_3 = 0$ ,  $y_2 = \frac{10}{9}$ , and  $y_1 = \frac{16}{9}$ . This is indicated in Fig. 3, where the dashed line near  $y_T = \frac{16}{9}$  represents the leading eigenvalue of  $B(n)$ .

The picture that thus emerges for generalized  $n$ -component cubic models is the following. The AT fixed line consists of a sequence of segments with an increasing degree of instability. The  $(k-1)$ -fold-unstable segment is separated from the  $k$ -fold-unstable segment by a multicritical point, say  $M_k$ . The cubic operator is marginal everywhere along the AT line. At  $M_k$  the exponent  $y_k$  changes sign, which results in a second marginal operator there. As  $n$  decreases from 2, a pair of  $k$ -

fold-unstable fixed points emerges from each  $M_k$ . The critical and low-temperature fixed points of the isotropic  $n$ -vector model constitute the onefold-unstable pair emerging from  $M_1$ , at which  $y_T=0$ ; the critical and tricritical Potts fixed points constitute the twofold-unstable pair emerging from  $M_2$ , at which  $y_T=\frac{3}{2}$ ; and new multicritical fixed points  $A(n)$  and  $B(n)$  form the threefold-unstable pair emerging from  $M_3$ , at which  $y_T=\frac{16}{9}$ . Similarly, additional  $k$ -fold-unstable fixed-point pairs will emerge from  $M_4, M_5$ , etc., at which  $y_T=\frac{15}{8}, \frac{48}{25}$ , etc. Thus the AT fixed line plays the role of a backbone for a hierarchy of pairs of fixed points of an increasing degree of instability.

### C. Numerical results and discussion

In this section we present the numerical RG results whose interpretation led to the conclusions described in Secs. III A and III B. Frequently we will contrast results for the pure and dilute  $n$ -component cubic models, (1.2) and (1.6), to demonstrate how the results of the calculation change when the parameter space is enlarged. Deviations of the numerical results from the ideal picture of Fig. 3 will also be discussed.

Consider first the  $2n$ -state Potts subspace  $P=0$  of the pure and dilute cubic models, (1.2) and (1.6), respectively. There the calculations reproduce previous work<sup>2</sup> such as the thermal critical and tricritical exponents as a function of  $n$ ; these results are shown as the dashed curves in Figs. 4(a) and 4(b). Only from the lattice-gas calculation does one obtain the correct changeover in the nature of the Potts phase transition from continuous at  $n \leq q_c/2$  to first order at  $n > q_c/2$ . The numerical critical value  $q_c/2 \approx 2.04$ , which is defined by the location of the tip of the dashed curve in Fig. 4(b), is close to Baxter's  $q_c/2=2$ .<sup>21</sup> The numerical exponents agree well with their exact values (3.1). For the dilute Potts model no critical fixed points were found for  $n < 0.7$ .<sup>2</sup> In the larger parameter space of the cubic model, i.e.,  $P \neq 0$ , one finds that the Potts critical fixed point is unstable under cubic anisotropy while the Potts tricritical and discontinuity fixed points are stable. The degree of instability is indicated in the figures by a number in parentheses next to the curves for the thermal exponents. Figure 5 exhibits the exponents associated with cubic anisotropy along the lines of Potts fixed points as obtained for the pure and dilute cubic models. The quality and internal consistency of the calculation for the lattice gas is indicated by the fact that the exponents associated with cubic anisotropy and dilution (for the latter, see Fig. 3 of Ref. 36) change sign at values close to one another and to  $q_c/2$ .

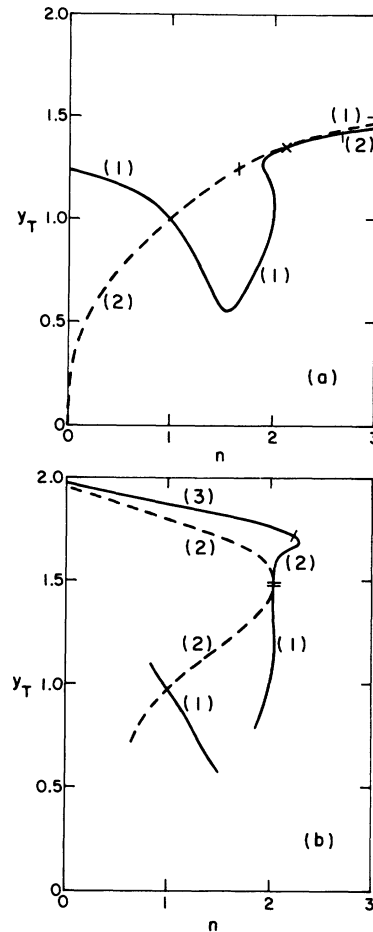


FIG. 4. Thermal exponents  $y_T$  vs  $n$  from the variational renormalization-group calculation for (a) the pure  $n$ -component cubic model and (b) the cubic lattice gas. The dashed curves indicate the critical and tricritical fixed points in the  $2n$ -state Potts subspace. The solid curves refer to isotropic  $n$ -vector, AT, and multicritical transitions. The degree of instability is shown by numbers in parentheses. The bars across the curves indicate change of stability. The  $\times$  symbol indicates the intersection of the  $2n$ -state Potts and AT lines of fixed points. The two horizontal bars in (b) near  $n=2, y_T=1.5$  give the interval in which (i) the Potts critical and tricritical fixed points coalesce, (ii) the AT and Potts lines of fixed points intersect, and (iii) one operator along the AT and two operators along the Potts fixed line change stability.

Next we discuss the cubic model in the regime  $n < 2$ . As function of  $n$ , the RG calculation yields, for the pure cubic model, a line of singly unstable fixed points in the sector  $P < 0$ . These fixed points are identified as governing a critical transition in the  $O_c(n)$  universality class. For the dilute cubic model one finds, in addition, a line of fixed points  $A(n)$  at

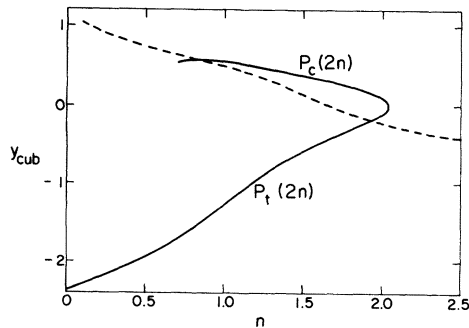


FIG. 5. Exponent associated with cubic symmetry breaking vs  $n$  along the lines of  $2n$ -state Potts fixed points as obtained from the variational renormalization group. The dashed and solid curves indicate results for the pure and dilute cubic models, respectively. The upper and lower branches of the solid curve give the critical and tricritical values of the exponents.

$P > 0$ , which are triply unstable. The thermal exponents are shown as solid curves in Figs. 4(a) and 4(b) and labeled singly (1) and triply (3) unstable, respectively. (For the dilute cubic model no critical fixed point is found when  $n \leq 0.8$ , as in the previous calculation<sup>2</sup> for the dilute Potts model, and when  $1.5 \leq n \leq 1.9$ . However, in these regimes dilution is unnecessary. For example, when the fixed points at either side of the latter interval are approached, the Boltzmann factors approach the pure fixed-point values. Fixed points in the gap can be found if negative fugacities are admitted.) There exist additional fixed points in the regime  $P > 0$ . They are, for the pure cubic model, the Ising  $I$  and  $n$ -state Potts  $P_c(n)$  fixed points and, for the cubic lattice gas, the Ising  $I$ , the critical, tricritical, and discontinuity  $n$ -state Potts  $P_c(n)$ ,  $P_t(n)$ ,  $P_d(n)$ , and critical-end-point CEP fixed points. The CEP is doubly unstable, with the leading exponent equal to the dimensionality. The location and stability of these fixed points leads to the phase diagrams of Figs. 2(a) and 1(a).

The results of the RG calculation for the thermal exponents of the pure and dilute AT model are given in Figs. 4(a) and 4(b) by the sharply rising solid curves near  $n = 2$ . An analysis shows the following. For the cubic lattice gas the thermal exponent increases as a function of the coupling constant from  $y_T \approx 0.78$  at  $P/C \approx -0.57$ , through the decoupled Ising point  $y_T = 1$  at  $P/C = -\frac{1}{2}$ , to the four-state Potts point  $y_T = 1.5$  at  $P/C = 0$ . We find that the singly unstable segment of the AT fixed line terminates almost precisely (to within 0.2%) at the point  $n = q_c/2$  at which the lines of critical and tricritical Potts fixed points  $P_c(2n)$  and  $P_t(2n)$  annihilate. Although this is expected, the accuracy ob-

tained by the approximate calculation is gratifying. For the pure cubic model the RG calculation approximates rather poorly the singly unstable segment of the AT fixed line, as shown in Fig. 4(a). It does produce a change in stability from onefold to twofold as expected, which it accomplishes by exchanging stability with the line of Potts fixed points  $P_c(2n)$  at  $n \approx 2.3$ . (The changes occur over a range of  $n$  values, in contrast to the calculation for the cubic lattice gas.) However, as discussed in Sec. II and Appendix A, the limited parameter space does not allow the correct description of the twofold unstable segment, which in turn is the reason for the poor approximation of the singly unstable one. As lines of fixed points cannot simply end in an analytic calculation, both AT and  $P_c(2n)$  continue on for all  $n$ . The former is located in the sector  $P > 0$ . The large- $n$  phase diagram that corresponds to this fixed-point structure would look like the one shown in Fig. 1(c), but all transitions would be found, incorrectly, to be continuous, with the single paramagnetic-to-ferromagnetic transition governed by the Potts and the bifurcation point governed by the double unstable "cubic" fixed point. This form of the phase diagram was found in earlier calculations.<sup>3,23</sup> Thus the fact that the parameter space is insufficient to permit first-order transitions has the result that the  $P_c(n)$  and AT fixed points play the role of the discontinuity and critical-end-point ones,  $P_d(2n)$  and CEP; these govern the cubic transition and bifurcation point in the lattice-gas calculation which implies the phase diagram of Fig. 1(c).

We return to the discussion of the dilute cubic model in the regime  $n \approx 2$ . The fixed line of the AT lattice gas is expected to extend beyond the four-state Potts point in a segment that is doubly unstable, with  $y_T$  in the interval  $\frac{3}{2} < y_T < \frac{16}{9}$ . Figure 4(b) shows the result of the RG calculation; the segment is obtained well, though with less precision than the singly unstable one. In the approximate treatment, the fixed points swing to values of  $n$  larger than 2, i.e., to about  $n = 2.3$ , and the change in stability occurs at  $n \approx 2.23$  above the tip at an exponent value  $y_T \approx 1.72$ , which is close to  $\frac{16}{9}$ . Along the AT fixed line there is one operator that is always marginal, while the other exponents are related to the thermal exponent by Eq. (3.4), with  $y_1 \equiv y_T$ . Figure 6 exhibits both the numerical and the exact results, which are shown as solid and dashed curves, respectively. For  $y_T \leq \frac{3}{2}$ , i.e., along the singly unstable segment, it is found that the cubic anisotropy exponent is zero to a very good approximation. The dilution exponent is irrelevant and poorly follows the exact value proportional to  $y_T$  with a slope of 4. At the multicritical point  $M_{k=2}$ , where  $y_T = \frac{3}{2}$ , the two next-to-leading exponents are found to exchange

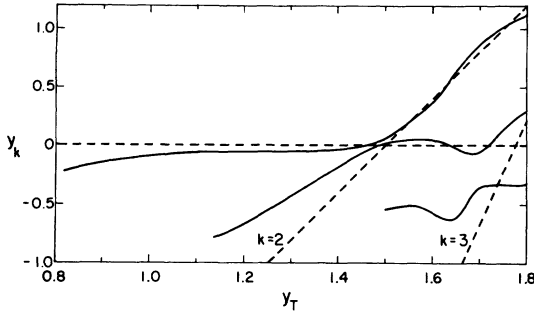


FIG. 6. Next-to-leading exponents along the extended AT fixed lines vs the leading exponent  $y_T$ . The dashed lines show the theoretical predictions for the marginal exponent  $y=0$ , and the exponents  $y_k$  given by Eq. (3.4) with  $y_1 \equiv y_T$ .

roles rather than to cross (not unlike a level splitting). Along the segment  $\frac{3}{2} < y_T < \frac{16}{9}$  the next-to-leading exponent  $y_2$ , now relevant, follows the exact value of Eq. (3.4) quite accurately. At  $M_{k=3}$ , where  $y_T = \frac{16}{9}$ , a similar phenomenon occurs, in that the third and fourth largest exponents seem to exchange roles. Finally, for the AT lattice gas tricritical behavior is found in the sector  $P < 0$ , but in contrast to the AT critical behavior it is universal and governed by the four-state Potts fixed point. When one ignores the inaccuracies of the numerical results, specifically the deviation from  $n=2$  of the doubly unstable segment of the AT fixed line, then the fixed-point structure found for  $n \approx 2$  leads to the phase diagram shown in Fig. 2(b). The intersection with the zero-fugacity plane yields the phase diagram of Fig. 1(b) for the pure AT model.

Now compare Figs. 4(a) and 4(b) with Fig. 3. One observes that the parameter space of the pure cubic model supports only the fixed points  $O_c(n)$ ,  $P_c(2n)$ , and part of the AT fixed line, while the parameter space of the cubic lattice gas supports, in addition, the fixed points  $P_t(2n)$ ,  $A(n)$ , and the full AT fixed line proper as well as the doubly unstable segment.

We turn to a discussion of various discrepancies between the results in Figs. 4(b) and 3, the latter of which are exact except for  $A(n)$  and  $B(n)$ . In this context we will also comment on the identification of the critical transition with the  $O(n)$  universality class. We note the following.

(1) The fact that, in our calculation, the AT fixed line and the line of isotropic fixed point  $O_c(n)$  do not meet at  $y_T=0$  for  $n \rightarrow 2^-$  is easily understood. We know that the fixed points  $O_g(n)$  are excluded from the parameter space of our calculation. The fixed points  $O_g(n)$  exist only in a rotationally invariant subspace. However, by its very construction,

our Hamiltonian space is not rotationally invariant but treats a discrete set of axes specially. An approximate calculation which includes both  $O_c(n)$  and  $O_g(n)$  is not difficult to envision. Its distinguishing feature is that it would describe an  $O(n)$  model in which the discrete perturbations could be turned on continuously in the form of symmetry-breaking fields, as for example in the calculation by José *et al.*<sup>31</sup>

(2) There are numerous arguments that support identifying the single paramagnetic-to-ferromagnetic phase transition of the cubic model with the universality class of the  $O(n)$  model. For the  $O(n)$  model in two dimensions cubic anisotropy is marginal, when  $n=2$ ,<sup>31</sup> and irrelevant when  $n < 2$ .<sup>32</sup> The equivalence of the transitions has been shown explicitly for special isotropic and cubic models.<sup>34,37</sup> For  $n < 1.6$ , the results for the thermal exponent by our numerical calculation are consistent with the exact values, though the agreement within 6% is far less impressive than in the case of the Potts exponents. The fact that the AT fixed line meets with the critical point of the planar model, for which  $y_T=0$ ,<sup>33</sup> was anticipated by Pfeuty and Toulouse<sup>38</sup> and has been derived recently through RG methods.<sup>28,29</sup>

(3) The AT fixed line and the line of  $2n$ -state Potts fixed points have the  $2n$ -state Potts fixed point in common. The comparison between Figs. 3 and 4(b) shows that this feature is very well described by the cubic-lattice-gas calculation. For the pure cubic model the RG approach does not produce this feature nearly as well, as seen from Fig. 4(a). By introducing dilution, one not only brings into the picture the doubly unstable segment of the AT fixed line, but also one achieves a convenient description of the disordered phase of the Potts model<sup>1,2</sup> (see also Appendix A). This makes it possible to describe within the approximate RG calculation also the first-order transition of the Potts model that takes place between disordered and ordered phases.

(4) Now compare Figs. 4(b) and 3 in the vicinity of the next multicritical point  $M_{k=3}$ , at which  $y_T = \frac{16}{9}$ . The dashed lines shown in Fig. 3 are missing in Fig. 4(b), and the results that are obtained are less accurate than those near the multicritical point  $M_{k=2} \equiv P(4)$ , at which  $y_T = \frac{3}{2}$ . One may conclude that enlarging the parameter space from the pure to the dilute  $n$ -component cubic model (1.6) has pushed the difficulties to the next level. In order to achieve more precision near the point  $M_{k=3}$  of the hierarchy of multicritical points, one must further enlarge the parameter space of the calculation, so as to bring into it the triply unstable segment of the AT fixed line as well as the line of fixed points  $B(n)$ . It is shown in Appendix A that this can be achieved in principle by introducing two lattice-gas variables:

The first dilutes the Potts spins  $a_i$  and then, at sites occupied by Potts spins, the second dilutes the Ising spins  $\sigma_i$ . This generalization incorporates into the calculation the equivalent of the Gaussian operator  $\cos(8\pi h)$ , which is responsible for the termination of the triply unstable segment of the AT fixed line. Owing to the large number of coupling and variational parameters in such a calculation (76 and 9, respectively) the search for fixed points is involved and has not been executed successfully.

Now we consider results for the  $n$ -component cubic lattice gas when  $n > 2$ . Figure 4(b) shows that no onefold unstable critical fixed points exist for  $n > 2$ . This implies that the cubic transition is first order for such  $n$ , i.e., in two dimensions  $n_c = 2$ . There exist twofold and threefold unstable fixed points out to  $n \approx 2.3$ , but we believe that their deviation from  $n = 2$  is an artifact of the calculation and that the face-cubic model does not exhibit any continuous transitions for  $n > 2$ . The fact that in our picture all fixed points annihilate in pairs at the AT fixed line necessitates a sharp division between continuous behavior for  $n \leq 2$  and first-order behavior for  $n > 2$ . This leads to the phase diagram of Fig. 2(c). For  $n > 2$ , the whole cubic transition surface is first order, governed by  $P_d(2n)$ , and only features on the sheets of  $n$ -state Potts and Ising transitions depend on the values of  $n$  and dilution. When  $n \rightarrow q_c = 4$  (in our approximation  $q_c \approx 4.08$ ), then the critical and tricritical fixed points on the Potts sheet also annihilate, so that for  $n > q_c$  the whole Potts sheet is governed by the first-order discontinuity fixed point  $P_d(n)$ .

Lastly, we comment on the nature of the transition between the partly and the fully ordered phases. The RG treatment presented here is biased in that it cannot yield a first-order transition between these two phases. A calculation permitting first-order transitions on both the  $n$ -state Potts and Ising sheets could employ the double dilution procedure mentioned earlier, in which the partially ordered phases can be characterized<sup>1,36</sup> by the spin state  $\sigma = 0$ . For details see the last three paragraphs of Appendix A. Then, for  $n > 2$ , the bifurcation of the cubic transition into  $n$ -state Potts and Ising transitions could have the character of an  $n$ -state Potts critical end point, or a triple point, or remain an Ising critical end point. The present calculation cannot rule out the first two possibilities.

#### D. Cubic model at $d > 2$

With the aid of the knowledge obtained above and a few additional exact results it is not difficult to discern several features of the evolution of the face-cubic model with dimensionality. First, one knows<sup>7</sup>

from expansions in  $d = 4 - \epsilon$  that the single paramagnetic-to-ferromagnetic transition is governed by the isotropic fixed point for  $n \leq n_c(d)$  and is first order for  $n > n_c(d)$ . For  $d \geq 4$ ,  $n_c = 4$ . Thus such transitions can be continuous when  $n < n_c(d)$ . However, the behavior of this transition at  $P = 0$ , which is that of the  $2n$ -state Potts model, is also known<sup>36,39,40</sup> and is continuous only for  $n \leq q_c(d)/2$  and first order for  $n > q_c(d)/2$ . For  $d \geq 4$ ,  $q_c(d) = 2$ .<sup>41</sup> It follows, therefore, that for values of  $n$  in the interval  $n_c(d) > n > q_c(d)/2$  the paramagnetic-to-ferromagnetic transition can either be critical, tricritical, or first order depending on the value of the coupling constant  $P/C$ .<sup>9</sup> The fixed point that governs the tricritical behavior is referred to as the cubic fixed point in the literature<sup>7</sup> and denoted  $C_f(n)$ , i.e., face-cubic, in the following discussion.

The comparison of the properties of the  $n$ -component cubic model for different values of dimension suggests that the AT fixed line evolves continuously into the line of doubly unstable cubic fixed points  $C_f(n)$ , when dimensionality is increased from 2. The graphs for the thermal exponents reflect this evolution. In Fig. 3 the thermal exponent along the AT fixed line is given by the vertical double line at  $n = 2$ . In an analogous figure for higher dimensions, the graph of the thermal exponent along  $C_f(n)$  would appear tilted, i.e.,  $y_T$  decreasing as a function of  $n$ . We have tested this relation between the line of fixed points  $C_f(n)$  at  $d > 2$  and the AT fixed line at  $d = 2$  by performing a variational RG calculation for the pure cubic model employing a lattice with five nearest neighbors,  $N = 2^d = 5$ , i.e., an effective dimensionality  $d \approx 2.32$ . The results are shown in Fig. 7. Comparison with Fig. 4(a) reveals the evolution with dimensionality. Cubic anisotropy is marginal in  $d = 2$  and relevant in  $d > 2$ ; therefore, the singly unstable segment of the AT fixed line evolves into a doubly unstable segment of the line of fixed points  $C_f(n)$ . The largest changes take place near two dimensions, which is consistent with the results that  $q_c(d)/2$  decreases<sup>36,39,40</sup> and  $n_c(d)$  increases<sup>9,32</sup> most rapidly for  $d \gtrsim 2$ . In particular,  $n_c$  changes from 2 in  $d = 2$  to approximately 3 in  $d = 2.32$ ,<sup>9,32</sup> with  $y_T \approx 0.4$ ,<sup>42</sup> and  $q_c$  changes from 2 in  $d = 2$  to approximately 2.8 in  $d = 2.32$ .<sup>36</sup> The latter result is exhibited in Fig. 7 by the tip of the dotted curve. This indicates the range of  $n$  over which in  $d = 2.32$  the line of twofold unstable cubic fixed points should exist. It would be interesting to perform an analogous calculation for the cubic lattice gas in  $d = 2.32$  dimensions, which would involve 39 coupling and 4 variational parameters. See Appendix B for details.

For  $d > 2$ , how do the lines of isotropic and Potts

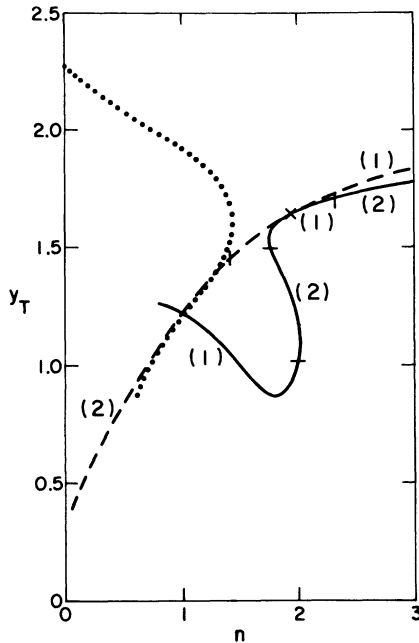


FIG. 7. Thermal exponent  $y_T$  vs  $n$  for the  $n$ -component cubic model in  $d=2.32$  dimensions from the variational renormalization-group calculation. Numbers in parentheses give the degrees of instability. The singly and doubly unstable portions of the solid curve for small  $n$  denote the exponent  $y_T$  along the lines of isotropic  $n$ -vector  $O_c(n)$  and cubic  $C_f(n)$  fixed points, respectively, while the dashed curve denotes the exponent  $y_T$  along the line of Potts transitions  $P_c(2n)$ . The analogous results for the same model in  $d=2$  dimensions are shown in Fig. 4(a). To indicate further the effect of the change in dimensionality, the results are complemented by data for the thermal critical and tricritical Potts exponents of Ref. 36 (dotted lines).

fixed points,  $O_c(n)$  and  $P_{c,t}(2n)$ , connect with the line  $C_f(n)$ ? The fixed points  $O_c(n)$  and  $C_f(n)$  are known to cross for some critical value  $n_c(d)$ , and at that point the respective thermal exponents as functions of  $n$  are tangential.<sup>9,43</sup> This feature is reminiscent of the behavior in two dimensions where  $y_T$  approaches zero like  $y_T \propto (2-n)^{1/2}$ .<sup>35</sup> Where and how the lines of cubic and Potts fixed points interconnect is not known; however, it is unlikely to occur precisely at  $q_c(d)/2$ .

The above picture has the following implication for the phase diagram of the cubic model in three dimensions, for which<sup>9</sup>  $n_c(3) \approx 3.4$  and<sup>36</sup>  $q_c(3)/2 \approx 1.1$ . For values of  $n$  such that  $q_c(3)/2 < n < n_c(3)$  the nature of the paramagnetic-to-ferromagnetic transition depends on the value of the coupling constant  $P/C$ .<sup>9</sup> Specifically, the three-dimensional Heisenberg model with face-cubic anisotropy and the three-dimensional AT model are

expected to exhibit single transitions that are continuous for sufficiently large and negative  $P$  and first order otherwise. For the case  $n=3$  this conclusion is in agreement with mean-field theory<sup>4</sup> in which the tricritical point occurs at  $P = -C/2$ . For the AT model, the conclusion agrees with mean-field theory as well as with the results of series analysis and Monte Carlo studies.<sup>44</sup>

#### IV. SUMMARY

We have investigated the family of phase transitions exhibited by the  $n$ -component cubic model in two dimensions. Several of our viewpoints differ from those of previous studies. The principle results are as follows.

(1) The investigation employs the vacancy technique. This allows one to describe within standard approximate RG calculations the continuous and first-order transitions of the cubic model and the fixed-line behavior of the AT model. We expect that the method will be useful for other investigations, such as clock models.

(2) The numerical RG results are interpreted with the aid of several exact results, some of which are new. In particular, the lattice-gas version of the AT model has been mapped onto the body-centered solid-on-solid model, and RG arguments have been used to generalize work by Kadanoff and Brown<sup>28</sup> and by Knops<sup>29</sup> relating the AT and Gaussian models. This mapping together with the numerical results of the variational RG shows that the AT line continues beyond the four-state Potts point as a doubly unstable line of nonuniversal bicritical points.

(3) The combination of our numerical and exact results suggests a unified picture of the phase transition occurring in generalized cubic models, one in which the extended AT fixed line plays a central role. In particular, at the special points on the AT fixed line where its stability changes and two operators are marginal, one of these operators is associated with the creation of a fixed-point pair as  $n$  decreases from 2. Of the pair that emerges as the AT line changes from  $(k-1)$ - to  $k$ -fold unstable, each fixed point is  $k$ -fold unstable. The critical and low-temperature fixed points of the isotropic  $n$ -vector model constitute the  $k=1$  pair, the  $2n$ -state Potts critical and tricritical fixed points constitute the  $k=2$  pair, and new multicritical points constitute the  $k=3$  pair.

(4) The successive calculations on the pure cubic and on the more general cubic lattice gas illustrate the general principle that the Hamiltonian space of an approximate RG calculation must be sufficiently large to permit description of the phenomena of in-

terest. The subspace of the pure cubic model is adequate for description of the transitions of the model for small  $n$  ( $n \lesssim 1.6$ ), but it is inadequate to describe the changes in the cubic and Potts transition with increasing  $n$ . The enlarged subspace of the cubic lattice gas is adequate to describe these phenomena but inadequate to provide a definitive description of, for example, the bifurcation point when  $n > 2$ . A larger subspace containing two dilution fields is needed to describe this, but it would surely fail in the description of other features and so on.

(5) The work has application to experimental systems. For example, it predicts that the face-cubic Heisenberg model ( $n = 3$ ) exhibits a first-order transition. Coupled with symmetry argument,<sup>11</sup> this predicts that the orientational ordering of  $N_2$  on graphite to a  $2 \times 1$  herringbone array will be first order, a prediction in agreement with the results of a recent Monte Carlo study.<sup>45</sup>

(6) The phase diagrams of the pure cubic model and the dilute lattice gas have been obtained and are summarized in the Introduction.

(7) With regard to dimensionality dependence, it appears that all properties such as  $q_c(d)$ ,  $n_c(d)$ , etc., evolve continuously with dimension. This observation coupled with our results for two dimensions permits us to draw conclusions about the cubic model in other dimensions, in particular the three-dimensional AT and Heisenberg models. These conclusions are in agreement with results of other calculations.

#### ACKNOWLEDGMENTS

We thank Kathie E. Newman for discussions and Alma Johnson for technical support. One of us (B.N.) received support from the National Science Foundation at the University of Chicago during the preparation of part of the manuscript. This research was supported in part by the National Science Foundation under Grant No. DMR-79-20785.

#### APPENDIX A: THE DILUTE ASHKIN-TELLER MODEL AND THE GAUSSIAN FIXED LINE

A relation between the AT critical behavior and the Gaussian model has been known for some time.<sup>28,29</sup> In this Appendix we review this connection<sup>29</sup> and generalize it to the dilute AT model. Our purpose is limited to understanding the effects of dilution. For more extensive information on the relation between the pure AT model and the Gaussian model we refer to the literature.<sup>28,29</sup>

In this Appendix we will use repeatedly the Kramers-Wannier duality transformation<sup>46,47</sup> for Ising variables, which can be written as

$$\tilde{W}_+ = W_+ + W_-, \quad \tilde{W}_- = W_+ - W_- \quad (\text{A1})$$

Here  $W_+$  and  $W_-$  are the Boltzmann weights in the original model for pairs of like and unlike nearest-neighbor spins, while  $\tilde{W}_+$  and  $\tilde{W}_-$  are the weights for the dual lattice. These Boltzmann weights may depend on other variables. Note also that if the original spins do not interact ( $W_+ = W_-$ ) then the dual variables are forced to be equal ( $\tilde{W}_- = 0$ ).

The pure AT Hamiltonian is

$$-\beta\mathcal{H} = \sum_{\langle i,j \rangle} [C(\delta_{a_i, a_j} \delta_{\sigma_i, \sigma_j} - 1) + P(\delta_{a_i, a_j} - 1)] \quad (\text{A2})$$

Both variables  $a$  and  $\sigma$  assume two values, which will be denoted as  $+1$  and  $-1$ . The dual transformation is applied to the  $\sigma$  variables. The resulting model has two sublattices, the original lattice  $L$  with variables  $a_i$  and the dual lattice  $D$  with variables  $\tilde{\sigma}_j$ . It is convenient to define this dual model by means of the Boltzmann weights for the elementary plaquettes consisting of two  $a$  and two  $\tilde{\sigma}$  variables. Four representative configurations are shown in Fig. 8(a). Their Boltzmann weights, in terms of the

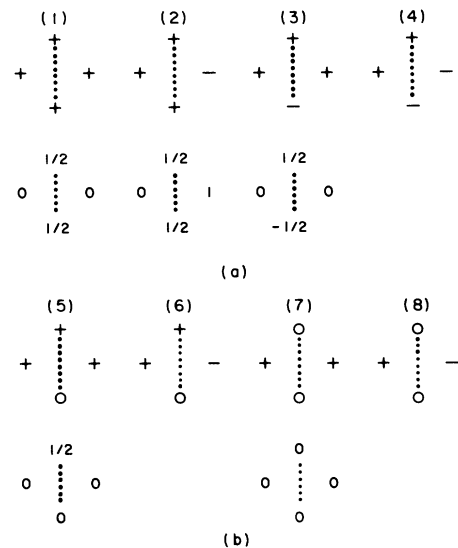


FIG. 8. (a) Basic configurations of a dual version of the pure Ashkin-Teller model and (b) additional configurations for the Ashkin-Teller lattice gas. The top rows give the values of the spin variables  $a$  and  $\tilde{\sigma}$  on plaquettes of original and dual lattice sites (top to bottom and left to right, respectively). The bottom row shows, for configurations with nonzero Boltzmann weights, the corresponding sets of column heights  $h$  in the equivalent body-centered solid-on-solid model.

weights of the original model, are

$$(\omega_1, \omega_2, \omega_3, \omega_4) \\ = (W_{\uparrow\uparrow} + W_{\uparrow\downarrow}, W_{\uparrow\uparrow} - W_{\uparrow\downarrow}, 2W_{\uparrow\rightarrow}, 0) . \quad (\text{A3})$$

All other configurations can be constructed by flipping simultaneously both  $a$  spins, or both  $\tilde{\sigma}$  spins, or all four spins. This model is now mapped onto a body-centered solid-on-solid (SOS) model<sup>48</sup> by identifying

$$a_i = \sin(\pi h_i) , \\ \tilde{\sigma}_j = \cos(\pi h_j) . \quad (\text{A4})$$

The variables  $h$  assume integer values on the sublattice  $D$  and half-integer values on  $L$  such that each nearest-neighbor pair of  $h$  differs by  $\frac{1}{2}$ . In Fig. 8(a) the values of  $h$  are given for the configurations of  $a$  and  $\tilde{\sigma}$  with nonzero Boltzmann weights. Apart from an overall additive constant the values  $h$  are uniquely determined by  $\tilde{\sigma}$  and  $a$ .

The discrete SOS model can be regarded as a continuous-variable model with strong fields that force the variables to assume their original discrete values. When these fields are irrelevant in the RG sense the model renormalizes to a Gaussian model.<sup>31</sup> When  $\omega_2 = \omega_3$ , the AT model is critical; the most relevant operator is

$$F_2 = \cos[2\pi(h_1 + h_2)] , \quad (\text{A5})$$

where the  $h_1$  and  $h_2$  occupy neighboring sites of  $L$  and  $D$ . Away from criticality there is also the operator conjugate to  $\omega_2 - \omega_3$ ,

$$F_1 = \cos[\frac{1}{2}\pi(h_1 + h_2 + h_3 + h_4)] , \quad (\text{A6})$$

where  $h_1, \dots, h_4$  occupy the corners of an elementary plaquette, as shown in Fig. 8(a). In the continuum, or Gaussian, limit the relevant behavior of  $F_1$  and  $F_2$  is given by

$$F_1 \propto \cos(2\pi h) , \quad F_2 \propto \cos(4\pi h) . \quad (\text{A7})$$

The exponents of these operators can be calculated in this limit and expressed in terms of the renormalized temperature of the Gaussian model  $T_G$ ,<sup>28,29</sup>

$$y_1 = 2 - T_G , \quad y_2 = 2 - 4T_G . \quad (\text{A8})$$

It follows that  $y_1 \leq \frac{3}{2}$  in the regime in which  $F_2$  is irrelevant. A consequence of this, for the phase diagram of the AT model, is the existence of a line of critical points, governed by the Gaussian model, along which the critical exponents vary continuously. As the thermal exponent  $y_1$  reaches  $\frac{3}{2}$  this critical line terminates since the presence of the now relevant operator  $F_2$  prevents further RG flows toward the Gaussian line. From other work one

knows that the critical line bifurcates into two Ising lines at this point.<sup>22</sup>

The above analysis indicates the features that are necessary for an approximate RG calculation to yield a qualitatively correct phase diagram for the AT model. Critical exponents that vary continuously are described by a *line* of fixed points. However, in an analytic RG transformation such a line cannot terminate. Therefore, a qualitatively correct picture can emerge only if the space of RG Hamiltonians is chosen large enough that it includes the continuation of the fixed line beyond the point at which it stops attracting flows from the AT model proper. In effect, this means that the Hamiltonian must include a free parameter with which one can change the coefficient of the operator  $F_2$  independently of those of additional relevant operators. We proceed by showing that dilution is such a parameter.

The Hamiltonian of the dilute AT model is

$$-\beta\mathcal{H} = \sum_{\langle i,j \rangle} t_i t_j [K + C(\delta_{a_i, a_j} \delta_{\sigma_i, \sigma_j} - 1) \\ + P(\delta_{a_i, a_j} - 1)] - \Delta \sum_i t_i . \quad (\text{A9})$$

Each site carries three variables:  $t_i = 0, 1$ ,  $a_i = \pm 1$ , and  $\sigma_i = \pm 1$ . Only when  $t_i = 1$  do the  $a_i$  and  $\sigma_i$  interact with their neighbors. Again a dual transformation is applied to  $\sigma$ . In addition to the Boltzmann weight of the pure AT model, i.e.,  $W_{\uparrow\uparrow}$ ,  $W_{\uparrow\downarrow}$ , and  $W_{\uparrow\rightarrow}$ , there are now weights  $W_{\uparrow 0}$  and  $W_{00}$  for states involving one or two vacant sites, which are denoted by the suffix 0. Likewise, in the dual model additional plaquette configurations appear, which are shown in Fig. 8(b). Only two of these have nonzero weight:

$$\omega_5 = 2W_{\uparrow 0} , \quad \omega_7 = 2W_{00} . \quad (\text{A10})$$

Now we identify

$$t_i a_i = \sin(\pi h_i) , \quad \tilde{\sigma}_j = \cos(\pi h_j) . \quad (\text{A11})$$

Note that the variable  $h$  now assumes integer values on  $D$  and both integer and half-integer values on  $L$ , so that nearest-neighbor pairs of  $h$  either are equal or differ by  $\frac{1}{2}$ . The Hamiltonian is extended by two new operators,

$$F'_1 = 1 - 2t_1 = \cos(2\pi h_1) , \\ F'_2 = (1 - 2t_1)(1 - 2t_2) \\ = \cos[2\pi(h_1 + h_2)] , \quad (\text{A12})$$

where  $h_1$  and  $h_2$  are nearest neighbors on  $L$ . Roughly, the operators  $F'_1$  and  $F'_2$  are conjugate to  $\Delta$  and  $K$ , respectively, as seen from Eq. (A9). There-

fore, by adjusting  $\Delta$  and  $K$  it is possible to make the coefficients of both  $\cos(2\pi h)$  and  $\cos(4\pi h)$  vanish. That is the initial condition for flows toward the segment of the Gaussian line where  $F_2$  is relevant and  $y_1 > \frac{3}{2}$ . Accordingly, an approximate RG in the space of dilute AT models will exhibit a fixed line with a singly and a doubly unstable segment. The point at which the two segments meet governs the termination of the fixed-line behavior in the space of the pure AT model. The doubly unstable segment attracts no flow from the pure subspace. Its presence in the space of Hamiltonians, however, is necessary to describe accurately in an approximate RG calculation the termination of the singly unstable segment.

As one follows the Gaussian line in the direction of increasing  $y_1$ , more and more operators become relevant.<sup>28,29</sup> The doubly unstable segment is terminated by the operator  $F_3$  becoming relevant,

$$F_3 = \frac{1}{2} \sum_{i=1}^4 \cos \left[ 2\pi \left( -h_i + \sum_{j=1}^4 h_j \right) \right] \\ = -t_1 - t_3 + 4t_1 t_3, \tag{A13}$$

with  $h_1, \dots, h_4$  on one elementary plaquette. The exponent of  $F_3$  is

$$y_3 = 2 - 9T_G, \tag{A14}$$

which becomes positive for  $y_1 > \frac{16}{9}$ . The parameters  $C, P, K,$  and  $\Delta$  in the Hamiltonian equation (A9) are sufficient to specify the temperature  $T_G$  and the coefficients of  $F_1, F_2,$  and  $F_3$  independently. Therefore, the space of dilute AT models contains also a triply unstable critical line with continuously varying exponents.

For completeness, we briefly discuss a further generalization. As explained above, dilution is introduced in order to invite the doubly unstable segment of the AT fixed line into the parameter space, thus allowing a correct and accurate description of the termination of the singly unstable segment. Another reason is that dilution makes possible the description of first-order transitions between ordered and disordered phases as discussed in Sec. II.<sup>1-3,36</sup> In a real space RG a first-order fixed point occurs at zero temperature. A disordered phase, however, is difficult to realize at  $T=0$ . Dilution allows an alternative description of the disordered phase, as an

TABLE I. Configurations of cubic spins. Spins are represented by a number, which labels the axis, and a sign, which symbolizes the direction along the axis. A small 0 signifies a vacancy. The first group of 21 configurations of four spins shows all classes for the dilute cubic model in  $d=2$  dimensions. The first 11 of those are the configurations without vacancies. The second group gives the 18 classes of configurations of five spins without vacancies for the cubic model in  $d=2.32$  dimensions, i.e.,  $N=5=2^d$ . For the corresponding dilute model the second group should be combined with the first group with an extra 0 added.

	$d=2$					$d=2.32$				
1	+1	+1	+1	+1	+1	+1	+1	+1	+1	+1
2	+1	+1	+1	-1	+1	+1	+1	+1	+1	-1
3	+1	+1	+1	+2	+1	+1	+1	+1	+1	+2
4	+1	+1	-1	-1	+1	+1	+1	+1	-1	-1
5	+1	+1	+2	+2	+1	+1	+1	+1	+2	+2
6	+1	+1	-1	+2	+1	+1	+1	+1	-1	+2
7	+1	+1	+2	-2	+1	+1	+1	+1	+2	-2
8	+1	+1	+2	+3	+1	+1	+1	+1	+2	+3
9	+1	-1	+2	-2	+1	+1	-1	-1	-1	+2
10	+1	-1	+2	+3	+1	+1	+2	+2	+2	-2
11	+1	+2	+3	+4	+1	+1	+2	+2	+2	+3
12	+1	+1	+1	0	+1	+1	-1	+2	+2	-2
13	+1	+1	-1	0	+1	+1	-1	+2	+2	+3
14	+1	+1	+2	0	+1	+1	+2	-2	+2	+3
15	+1	-1	+2	0	+1	+1	+2	+3	+2	+4
16	+1	+2	+3	0	+1	-1	+2	-2	+2	+3
17	+1	+1	0	0	+1	-1	+2	+3	+2	+4
18	+1	-1	0	0	+1	+2	+3	+4	+2	+5
19	+1	+2	0	0						
20	+1	0	0	0						
21	0	0	0	0						

empty phase, which has the same symmetry, but poses no difficulties at  $T=0$ .

In the cubic and AT models there are three phases—ordered, disordered, and partially ordered—and correspondingly three phase transitions. In the dilute models the vacancy is used to describe the disordered phase, while the cubic spin states describe the  $2n$  equivalent ordered phases, but there is no single state that describes the partially ordered phase. As a consequence, an RG treatment of these models will always yield a second-order transition from the partially to the fully ordered phase. To examine whether this is correct one should introduce a state that allows one to describe the partially ordered phases. Since in this phase  $a$  is ordered, in any of its  $n$  states, and  $\sigma$  is disordered, the natural choice is  $\sigma=0$ . The number of sites with  $\sigma=0$  can be controlled by a new chemical potential in addition to  $\Delta$ . Therefore, in this generalization lattice sites are either completely vacant, occupied by  $a$  and  $\sigma$  ( $a, \sigma = \pm 1$ ) or by  $a$  alone ( $a = \pm 1, \sigma = 0$ ). The latter states will be indicated symbolically by a short vertical or horizontal line,  $|$  or  $-$ . The Boltzmann weights for nearest-neighbor pairs are  $W_{\uparrow\uparrow}$ ,  $W_{\uparrow\downarrow}$ ,  $W_{\downarrow\uparrow}$ ,  $W_{\downarrow\downarrow}$ ,  $W_{\uparrow|}$ ,  $W_{\uparrow-}$ ,  $W_{\downarrow|}$ ,  $W_{\downarrow-}$ ,  $W_{|0}$ , and  $W_{00}$ . Since the Hamiltonian is rather unwieldy, we use these weights to define the parameter space.

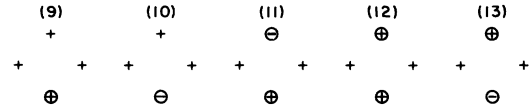


FIG. 9. Configuration of a dual version of the doubly dilute Ashkin-Teller lattice gas. The symbols  $\oplus$  and  $\ominus$  denote  $|\sigma|=0$  with  $a=+1$  and  $-1$ , respectively.

Applying a dual transformation to the sign of  $\sigma$  yields the configurations of Fig. 8, with weights as in (A3) and (A10), and in addition the configurations shown in Fig. 9, with the weights

$$\omega_9 = 2W_{\uparrow|}, \quad \omega_{10} = 2W_{\uparrow-}, \quad \omega_{11} = 2W_{|0}, \quad (A15)$$

$$\omega_{12} = 2W_{||}, \quad \omega_{13} = 2W_{|-}.$$

The new states with  $\sigma=0$  can be accommodated by introducing additional values of  $h$ ,

$$t_i a_i \left[ \frac{t_i + |\sigma_i|}{2} \right]^{1/2} = \sin(\pi h_i), \quad \tilde{\sigma}_j = \cos(\pi h_j). \quad (A16)$$

TABLE II. Fixed points of the variational renormalization group for the  $n=1$  component cubic model in  $d=2$  and in  $d=2.32$  dimensions. The values of the logarithms of the variational weights  $P_{\uparrow\uparrow}$  and  $P_{\uparrow\downarrow}$ , and of the Boltzmann weights of the configurations of four ( $d=2$ ) and five ( $d=2.32$ ) cubic spins are given at the fixed points  $O_c(1)$  and  $P_c(2)$ . The numbering of the configurations corresponds to that in Table I.

	$d=2$		$d=2.32$	
	$O_c(1)$	$P_c(2)$	$O_c(1)$	$P_c(2)$
$\ln P_{\uparrow\uparrow}$	-1.5717	-1.5717	-1.2086	-1.2086
$\ln P_{\uparrow\downarrow}$	-0.7712	-1.5717	-0.5827	-1.2086
1	-0.0558	-0.0558	-0.0889	-0.0888
2	-0.8803	-0.8803	-0.6569	-0.6569
3	-0.4680	-0.8803	-0.3432	-0.6569
4	-1.1735	-1.1735	-0.9504	-0.9504
5	-0.6146	-1.1735	-0.4648	-0.9504
6	-1.0368	-1.3274	-0.7942	-1.0014
7	-0.8894	-1.3274	-0.6409	-1.0014
8	-0.7428	-1.3274	-0.5495	-1.0014
9	-1.1530	-1.4725	-0.9484	-1.1064
10	-1.0177	-1.4725	-0.7884	-1.1064
11	-0.8695	-1.4725	-0.6163	-1.1064
12			-0.9527	-1.1600
13			-0.8676	-1.1600
14			-0.7873	-1.1600
15			-0.6986	-1.1600
16			-0.9515	-1.2119
17			-0.8665	-1.2119
18			-0.7795	-1.2119

TABLE III. Fixed points of the variational renormalization group for the  $n=1$  component cubic lattice gas in  $d=2$  dimensions. The values of the logarithms of the variational weights  $P_{11}$ ,  $P_{1\rightarrow}$ ,  $P_{10}$ , and  $P_{00}$  and of the Boltzmann weights of the configurations of four cubic spins are given at the fixed points  $O_c(1)$ ,  $P_c(2)$ ,  $P_t(2)$ , and  $A(1)$ . The numbering of configurations corresponds to that in Table I.

	$O_c(1)$	$P_c(2)$	$P_t(2)$	$A(1)$
$\ln P_{11}$	-2.1897	-2.1897	-5.9658	-1.6893
$\ln P_{1\rightarrow}$	-0.8335	-2.1897	-5.9658	-9.6069
$\ln P_{10}$	-0.8272	-1.2602	-1.5145	-1.6893
$\ln P_{00}$	-0.6107	-1.4767	-0.1190	-0.0
1	-0.1596	-0.1596	-0.0642	-0.0615
2	-1.1334	-1.1334	-2.6780	-1.0631
3	-0.5486	-1.1334	-2.6780	-3.4879
4	-1.5538	-1.5538	-3.5805	-1.4306
5	-0.6590	-1.5538	-3.5805	-4.8142
6	-1.3152	-1.8264	-3.8727	-3.6574
7	-1.1284	-1.8264	-3.8727	-4.8225
8	-0.8682	-1.8264	-3.8727	-5.1482
9	-1.5268	-2.1423	-4.2791	-4.8301
10	-1.3089	-2.1423	-4.2791	-5.1599
11	-1.0659	-2.1423	-4.2791	-5.6525
12	-0.6853	-0.6853	-0.8640	-1.0631
13	-1.4688	-1.4688	-2.5473	-1.5436
14	-1.0097	-1.4688	-2.5473	-3.3540
15	-1.4615	-1.8437	-3.0803	-3.3850
16	-1.2115	-1.8437	-3.0803	-4.0583
17	-1.1529	-1.1529	-1.1398	-1.4305
18	-1.6156	-1.6156	-1.9322	-1.5436
19	-1.3586	-1.6156	-1.9322	-2.5074
20	-1.5068	-1.5068	-0.8790	-1.0631
21	-1.6555	-1.6555	-0.1368	-0.0615

Now  $h$  is integer on the sublattice  $D$  and integer, half-integer, and integer divided by 4 on the sublattice  $L$ . The large parameter space makes accessible a host of new fields; in particular, the operator  $F_4 = \cos(8\pi h)$  that is conjugate to the new chemical potential which governs the new allowed  $h$  values.

#### APPENDIX B: LOWER-BOUND RENORMALIZATION GROUP FOR CUBIC MODELS

In this Appendix we present some technical details on the numerical methods used to study the cubic model. The purpose is to aid the reader who wishes to conduct an investigation that is similar to or generalizes the study reported here.

The Kadanoff variational RG (Ref. 30) is designed such that it yields a lower bound to the free energy. A few free parameters are utilized to maximize this bound. In general the optimization requires the solution of extremely unwieldy equations, but at a fixed point these simplify dramatically. Therefore, in most calculations the optimization is

performed only at the fixed point. The critical exponents follow as usual from the derivative of the RG transformation. This derivative is evaluated while keeping the variational parameters constant at the value that optimizes the fixed-point free energy. This somewhat inconsistent procedure<sup>49</sup> has been shown to yield extremely accurate critical exponents for reasons that are not understood. The same method is followed in this paper. It should be noted that the results consist solely in critical exponents, because the evaluation of phase diagrams or thermodynamic functions would require RG flows and hence optimization away from fixed points. Such flows, though possible in principle, tend to demand much computer time. In practice, phase diagrams are derived qualitatively from the location and relative stability of the various fixed points and their evolution with the number of spin components.

The Kadanoff variational RG equations were developed for spin models on a  $d$ -dimensional hypercubic lattice. The Hamiltonian is written as a sum of local Hamiltonians  $-\beta\mathcal{H} = \sum H_{hc}$ , each in-

volution of the  $N=2^d$  sites of an elementary hypercube. The basic RG transformation reads

$$W'(s'_1, s'_2, \dots, s'_N) = \sum_{\{s\}} \frac{W(s_1, s_2, \dots, s_N)^N \prod_{i=1}^N V(s_i, s'_i; P)}{\sum_{\sigma} \prod_{i=1}^N V(s_i, \sigma; P)}. \quad (\text{B1})$$

The  $W$  are the Boltzmann weights (BW) as functions of the original spins  $s_i$  and the  $W'$  are the renormalized BW as functions of the new spins  $s'_i$ . The function  $V$  is a two-spin coupling between a new and an old spin determined by a set of variational parameters  $P$ . For example, for the cubic lattice gas (1.6) in two dimensions one may use

$$V \propto \exp \left[ \sum_{i=1}^4 t_i t' [p_1 + \delta_{a_i, a'} (p_2 + p_3 \delta_{\sigma_i, \sigma'})] + p_4 (t_i + t') \right].$$

However, the discussion in this Appendix is more general. In Eq. (B1) the sum in the numerator is over all possible configurations of the  $N$  old spins, while the denominator is summed over the states of a single spin coupled to  $N$  new spins. Not all the different configurations on the hypercube will have different energies. Two different configurations have the same BW if they can be transformed into one another by a rotation in spin space or by a permutation of the  $N$  arguments. Thus BW are associated with classes of equivalent configurations. For the pure and dilute cubic models these classes are each represented by a member configuration in Table I for  $N=4$  (i.e.,  $d=2$ ) and 5 (i.e.,  $d \approx 2.32$ ). The parameter space of the local Hamiltonians  $H_{\text{hc}}$  is parametrized by the BW of these classes. Like-

wise, the coupling between the old and new spins is parametrized by means of the BW of two spins:  $P_{\uparrow\uparrow}$ ,  $P_{\uparrow\rightarrow}$ ,  $P_{\uparrow 0}$ , and  $P_{00}$ , keeping  $P_{\uparrow\uparrow} = 1$ .

With these definitions (B1) can be written

$$W'_\mu = \sum_\nu \frac{R_{\mu\nu}}{Q_\nu} W_\nu^N, \quad (\text{B2})$$

where the indices  $\mu$  and  $\nu$  signify the equivalence classes of configurations of  $\{s'\}$  and  $\{s\}$ , respectively, and

$$Q_\nu = \sum_\sigma \prod_{i=1}^N V(s_i, \sigma; P) \text{ with } \{s\} \in \nu, \quad (\text{B3})$$

$$R_{\mu\nu} = \sum_{\{s'\} \in \nu} \prod_{i=1}^N V(s_i, s'_i; P) \text{ with } \{s'\} \in \mu. \quad (\text{B4})$$

Thus the fixed-point equation

$$B_\mu = \sum_\nu \frac{R_{\mu\nu}}{Q_\nu} B_\nu^N \quad (\text{B5})$$

must be solved simultaneously with the optimization equation

$$\sum_{\mu, \nu} W_\mu^N M_\mu Q_\mu^{-1} W_\nu^N \frac{\partial}{\partial P_\alpha} \frac{R_{\mu\nu}}{Q_\nu} = 0. \quad (\text{B6})$$

Here  $P_\alpha$  stands for the set  $P_{\uparrow\uparrow}$ ,  $P_{\uparrow\rightarrow}$ ,  $P_{\uparrow 0}$ , and  $P_{00}$ .  $M_\mu$  is the multiplicity of  $\mu$  or the number of configurations in class  $\mu$ . For example,  $M_\mu$  for the first three classes listed in Table I is  $2n$ ,  $2nN$ , and  $4n(n-1)N$ , respectively.

In practice, Eqs. (B5) and (B6) are solved by first choosing a particular value of  $n$  for which the system reduces to a simple model. This fixed point is then followed as a function of  $n$  by changing  $n$  in small steps and using the previous fixed-point coordinates as a first guess. In Tables II and III we list the values of  $W$  and  $P$  at various fixed points for  $n=1$ .

\*Present address: Philips Natuurkundig Laboratorium, Postbus 8000, 5600 JA Eindhoven, The Netherlands.

†Corresponding author.

<sup>1</sup>B. Nienhuis, A. N. Berker, E. K. Riedel, and M. Schick, Phys. Rev. Lett. **43**, 737 (1979).

<sup>2</sup>B. Nienhuis, E. K. Riedel, and M. Schick, J. Phys. A **13**, L31 (1980); T. W. Burkhardt, Z. Phys. B **39**, 159 (1980).

<sup>3</sup>Preliminary results have been previously reported by E. K. Riedel, Physica (Utrecht) **106A**, 110 (1981).

<sup>4</sup>D. Kim, P. M. Levy, and L. F. Uffer, Phys. Rev. B **12**, 989 (1975); D. Kim, P. M. Levy, and J. J. Sudano, *ibid.*

**13**, 2054 (1976).

<sup>5</sup>R. B. Potts, Proc. Cambridge Philos. Soc. **48**, 106 (1952). For a review, see F. Y. Wu, Rev. Mod. Phys. **54**, 235 (1982).

<sup>6</sup>J. Ashkin and E. Teller, Phys. Rev. **64**, 178 (1943).

<sup>7</sup>See A. Aharony, in *Phase Transitions and Critical Phenomena*, edited by C. Domb and M. S. Green (Academic, London, 1976), Vol. 6.

<sup>8</sup>E. Domany and E. K. Riedel, Phys. Rev. B **19**, 5817 (1979).

<sup>9</sup>K. E. Newman and E. K. Riedel, Phys. Rev. B **25**, 264

- (1982).
- <sup>10</sup>For a review, see M. Schick, *Surf. Sci.* **125**, 94 (1983).
- <sup>11</sup>A. B. Harris and A. J. Berlinsky, *Can. J. Phys.* **57**, 1852 (1979).
- <sup>12</sup>T. T. Chung and J. G. Dash, *Surf. Sci.* **66**, 559 (1977); J. Eckert, W. D. Ellenson, J. B. Hastings, and L. L. Passell, *Phys. Rev. Lett.* **43**, 1329 (1979); R. D. Diehl, M. F. Toney, and S. C. Fain, Jr., *Surf. Sci.* **125**, 116 (1983).
- <sup>13</sup>E. Domany and E. K. Riedel, *Phys. Rev. Lett.* **40**, 561 (1978).
- <sup>14</sup>J. P. McTague and M. Nielsen, *Phys. Rev. Lett.* **37**, 596 (1976). However, evidence that the  $O_2$  is not in a triangular array in the disordered phase is presented by P. W. Stephens, P. A. Heiney, R. J. Birgeneau, P. M. Horn, J. Stoltenberg, and O. E. Vilches, *Phys. Rev. Lett.* **45**, 1959 (1980).
- <sup>15</sup>E. Domany, M. Schick, J. S. Walker, and R. B. Griffiths, *Phys. Rev.* **18**, 2209 (1978).
- <sup>16</sup>M. G. Lagally, T.-M. Lu, and G.-C. Wang, in *Ordering in Two Dimensions*, edited by S. Sinha (Elsevier, New York, 1980), p. 113.
- <sup>17</sup>E. Domany, M. Schick, and J. S. Walker, *Phys. Rev. Lett.* **38**, 1148 (1977).
- <sup>18</sup>M. J. Tejwani, O. Ferreira, and O. E. Vilches, *Phys. Rev. Lett.* **44**, 152 (1980).
- <sup>19</sup>P. G. de Gennes, *Phys. Lett.* **38A**, 339 (1972).
- <sup>20</sup>R. Vilanova and F. Rondelez, *Phys. Rev. Lett.* **45**, 1502 (1980).
- <sup>21</sup>R. J. Baxter, *J. Phys. C* **6**, L445 (1973).
- <sup>22</sup>F. J. Wegner, *J. Phys. C* **5**, L131 (1972); F. Y. Wu and K. Y. Lin, *ibid.* **7**, L181 (1974); H. J. F. Knops, *J. Phys. A* **8**, 1508 (1975).
- <sup>23</sup>A. Aharony, *J. Phys. A* **10**, 389 (1977); M. P. M. den Nijs, *Physica (Utrecht)* **95A**, 449 (1979).
- <sup>24</sup>J. L. Black and V. J. Emery, *Phys. Rev. B* **23**, 429 (1981); B. Nienhuis, *J. Phys. A* **15**, 199 (1982).
- <sup>25</sup>M. P. M. den Nijs, *J. Phys. A* **12**, 1857 (1979).
- <sup>26</sup>L. P. Kadanoff, *Phys. Rev. Lett.* **39**, 903 (1977).
- <sup>27</sup>L. P. Kadanoff and F. J. Wegner, *Phys. Rev. B* **4**, 3989 (1971).
- <sup>28</sup>L. P. Kadanoff, *Ann. Phys. (N.Y.)* **120**, 39 (1979); L. P. Kadanoff and A. C. Brown, *ibid.* **121**, 318 (1979).
- <sup>29</sup>H. J. F. Knops, *Ann. Phys. (N.Y.)* **128**, 448 (1980); H. J. F. Knops and L. W. J. den Ouden, *ibid.* **138**, 155 (1982).
- <sup>30</sup>L. P. Kadanoff, *Phys. Rev. Lett.* **34**, 1005 (1975). For a review of the method, see T. W. Burkhardt, in *Real-Space Renormalization*, edited by T. W. Burkhardt and J. M. J. van Leeuwen (Springer, New York, 1982), Chap. 2.
- <sup>31</sup>J. José, L. P. Kadanoff, S. Kirkpatrick, and R. D. Nelson, *Phys. Rev. B* **16**, 1217 (1977).
- <sup>32</sup>R. A. Pelcovits and D. R. Nelson, *Phys. Lett.* **57A**, 23 (1976).
- <sup>33</sup>That the  $O_c(n)$  fixed point meets the AT line can be seen from the following consideration. Setting  $W_{11}=0$  in a triangular AT model prohibits vortices and thus reduces the model to a solid-on-solid model. The AT line intersects this solid-on-solid line at the transition point, which is identical to the critical point of the  $O(2)$  model by duality. See also Y. Stavans and E. Domany, *Phys. Rev. B* **27**, 3043 (1983).
- <sup>34</sup>B. Nienhuis, *Phys. Rev. Lett.* **49**, 1062 (1982).
- <sup>35</sup>For an earlier conjecture of the results of Eq. (3.2), see J. L. Cardy and H. W. Hamber, *Phys. Rev. Lett.* **45**, 499 (1980).
- <sup>36</sup>B. Nienhuis, E. K. Riedel, and M. Schick, *Phys. Rev. B* **23**, 6055 (1981).
- <sup>37</sup>E. Domany, D. Mukamel, B. Nienhuis, and A. Schwimmer, *Nucl. Phys. B* **190**, [FS3], 279 (1981).
- <sup>38</sup>P. Pfeuty and G. Toulouse, *Introduction to the Renormalization Group and to Critical Phenomena* (Wiley, New York, 1977).
- <sup>39</sup>J. B. Kogut and D. K. Sinclair, *Phys. Lett.* **86A**, 38 (1981).
- <sup>40</sup>K. E. Newman, E. K. Riedel, and S. Muto (unpublished).
- <sup>41</sup>A. Aharony and E. Pytte, *Phys. Rev. B* **23**, 362 (1981).
- <sup>42</sup>S. Hikami and E. Brézin, *J. Phys. A* **11**, 1141 (1978).
- <sup>43</sup>A. Aharony, *Phys. Rev. B* **8**, 4270 (1973).
- <sup>44</sup>R. V. Ditzian, J. R. Banavar, G. S. Grest, and L. P. Kadanoff, *Phys. Rev. B* **22**, 2542 (1980).
- <sup>45</sup>O. G. Mauritsen and A. J. Berlinsky, *Phys. Rev. Lett.* **48**, 181 (1982).
- <sup>46</sup>K. A. Kramers and G. H. Wannier, *Phys. Rev.* **60**, 252 (1941).
- <sup>47</sup>F. Y. Wu and Y. K. Wang, *J. Math. Phys.* **17**, 439 (1976).
- <sup>48</sup>H. van Beijeren, *Phys. Rev. Lett.* **38**, 993 (1977).
- <sup>49</sup>W. van Saarloos, J. M. J. van Leeuwen, and A. M. M. Pruisken, *Physica (Utrecht)* **92A**, 323 (1978); M. P. M. den Nijs and H. J. F. Knops, *ibid.* **93A**, 441 (1978).